2002 were utilized to calculate the S parameters of the band-selective filter. The S parameters of the proposed circuits in this study were measured by using an Agilent E8362B PNA series network analyzer. Figures 3 and 4 show a comparison of the simulated and measured S parameters of the CPW band-selective filter. The pass-band responses operated below 2.6 GHz and from 5.0 to 6.0 GHz. Figure 5 shows the LC-equivalent model of the proposed filter. The values of the lumped elements are analyzed and calculated by utilizing the transmission line model. Table 1 presents the equivalent lumped-element values from the approximate *L–C* values and optimized *L–C* values. Figure 6 shows the comparison of the measured reflection coefficients of the CPW-fed spiral slot antenna and one integrated with the CPW band-selective filter. The antenna module covers the frequency bands of the wireless communication systems and filters out the out-of-band signals, so that the received noise can be suppressed and the noise figure can be reduced. Figure 7 presents the measured radiation patterns of the *E* and *H* planes of the slot antenna at 1.8, 2.4, 5.2, and 5.8 GHz. The power intensity of the cross-polarization radiations of the CPW-fed antennas was similar to one of the copolarization radiations. This phenomenon may be attributed to the enhancement of the surface wave because of the CPW feeding structure and the spiral radiation aperture of the antenna. The irregular radiation patterns measured at 5.2 and 5.8 GHz showed that the power leakage was due to a combination of the dominant, traveling, and surface-wave modes. The measured antenna gain was about 1.75 dB at 1.8 GHz.

4. CONCLUSION

In this study, a CPW-fed band-selective filter is demonstrated for the use of the wideband spiral slot antenna. By placing the band-selective filter between the wideband antenna and low noise amplifier, the out-of-band signals are rejected such that the noise figure of the communication systems could be reduced. This design of the CPW antenna module can be useful for the monolithic microwave integrated circuit.

REFERENCES

1. C.J. Wang, C.H. Lin, and J.W. Wu, A microstrip filter utilized in ultra-wideband antennas, Microwave and Opt Technol Lett 41 (2004), 248–251.
2. F.L. Lin and R.B. Wu, Computations for radiation and surface-wave losses in coplanar waveguide bandpass filters, IEEE Trans Microwave Theory Techn 47 (1999), 385–389.
3. Y.K. Kuo, C.H. Wang, and C.H. Chen, Novel reduced-size coplanar-waveguide bandpass filters, IEEE Microwave Wireless Components Lett 11 (2001), 65–67.
4. A. Görür and Ö. Akgün, Resonance characteristics of capacitively loaded CPW open-loop resonators, Microwave Opt Technol Lett 38 (2003), 298–300.
5. J.W. Bandler, R.M. Biernacki, S.H. Chen, D.G. Swanson, Jr., and S.Ye, Microstrip filter design using direct EM field simulation, IEEE Trans Microwave Theory Tech 42 (1994), 1353–1359.
6. S.S. Liao, H.K. Chen, Y.C. Chang, and K.T. Li, Novel reduced-size coplanar waveguide bandpass filter using the new folded open stub structure, IEEE Microwave Wireless Components Lett 12 (2002), 476–478.

DISTRIBUTED HYBRID-FIBER RAMAN AMPLIFIERS WITH A SECTION OF NONLINEAR MICROSTRUCTURED OPTICAL FIBER

Yan-ge Liu, Chao Wang, Tingting Sun, Yan Li, Zhi Wang, Chunshu Zhang, Guiyun Kai, and Xiaoyi Dong
Key Laboratory of Opto-Electronic Information Science and Technology
Ministry of Education, Institute of Modern Optics
Nankai University
Tianjin 300071, China

Received 30 March 2006

ABSTRACT: *A distributed hybrid-fiber Raman amplifier with a 25-km single-mode fiber and a section of nonlinear microstructured optical fiber (NMOF) is proposed and experimentally investigated in detail. Three pump schemes and span configurations, as well as two NMOF types with different parameters and length were considered. The influence of the NMOF presence on the performance of the amplifier was analyzed.* © 2006 Wiley Periodicals, Inc. Microwave Opt Technol Lett 48: 2267–2271, 2006; Published online in Wiley InterScience (www.interscience.wiley.com). DOI 10.1002/mop.21901

Key words: *fiber Raman amplifiers; microstructured optical fiber (MOF); photonic crystal fiber (PCF)*

1. INTRODUCTION

Microstructured optical fibers (MOFs), also called photonic crystal fibers (PCFs), have attracted considerable interest in recent years due to their unique characteristics such as endlessly single-mode property [1], highly effective nonlinearity [2], and controllable dispersion property [3]. Such fibers consist of a pure silica core surrounded by a regular array of longitudinal air holes and can be designed to have effective mode area A_{eff} at least as small as 1.7 μm^2 at 1550 nm [4]. Hence, they can provide an effective nonlinearity per unit length which can be an order or more higher than that of a conventional fiber. The enhanced nonlinear properties of MOFs can be exploited for Raman amplification [5–8]. A continuous-wave pumped Raman laser [5], as well as an L^+-band Raman amplifier [6] in a PCF, have already been experimentally demon-

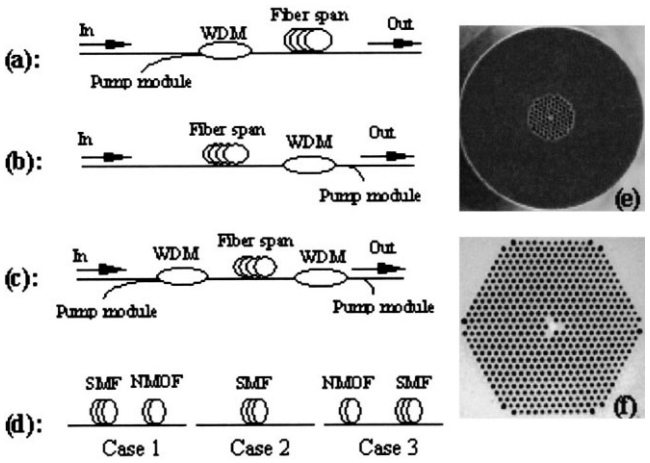

Figure 1 Experimental setup: (a) forward-pumped configuration, (b) backward-pumped configuration, (c) bidirectional-pumped configuration, (d) fiber configuration of the span, (e) and (f) is the transverse structure of NMOF1 and NMOF2

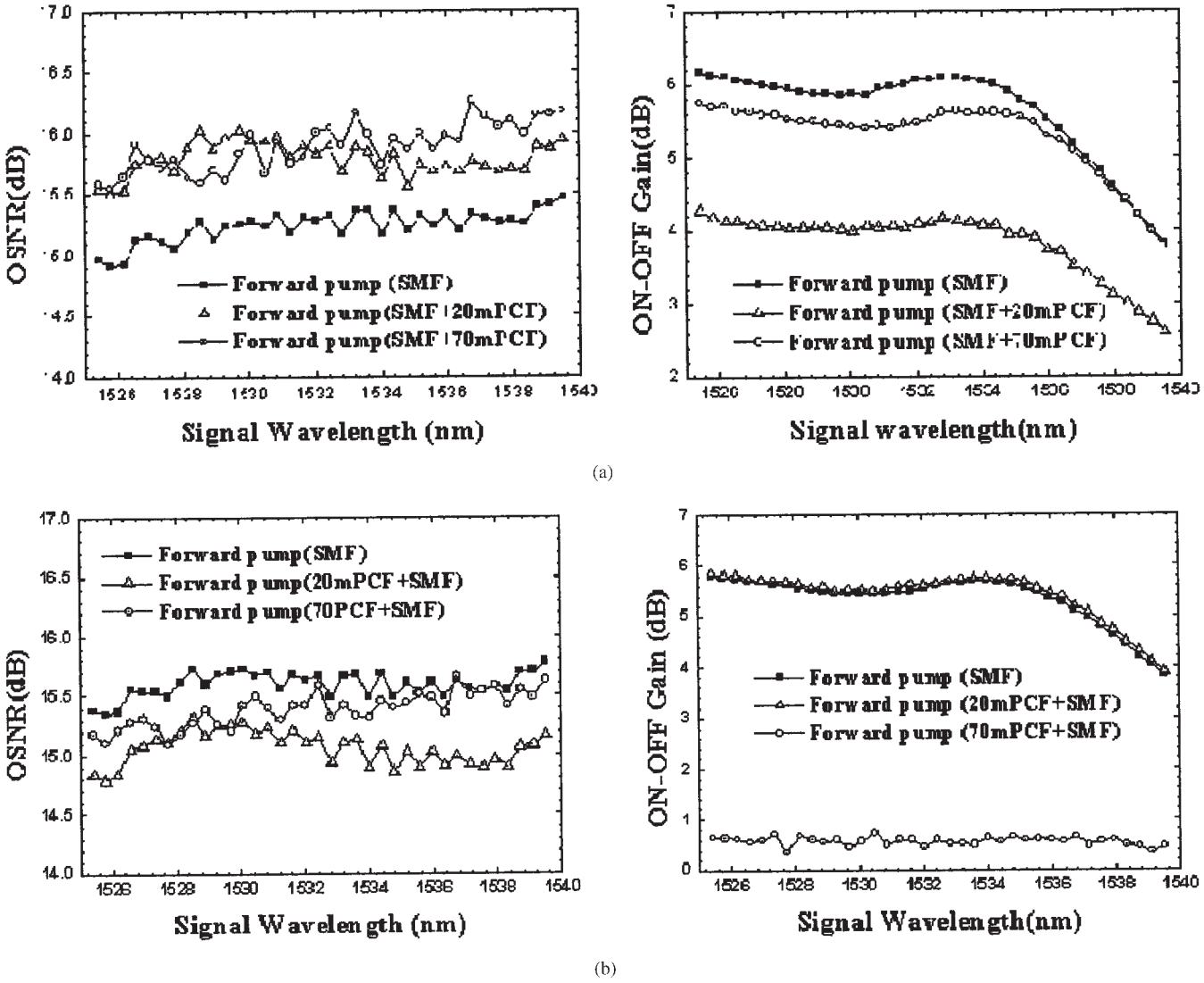

Figure 2 (a) Performance comparison between Case 1 and Case 2 for the forward-pumped configuration (the pump power is 365 mW). (b) Performance comparison between Case 3 and Case 2 for the forward-pumped configuration (the pump power is 327 mW)

strated. Moreover, the Raman properties of triangular air hole lattice PCFs with/without a germania-doped core have been theoretically investigated [7]. An accurate model that combines the calculation of the Raman gain coefficient and the solution of the Raman propagation equations has also been developed to study PCF Raman amplifiers [8]. In those Raman amplifiers, the PCF is all used as the one and only gain medium.

In this paper, a detailed experimental investigation on the hybrid-distributed fiber Raman amplifier (HFRA) consisting of a 25-km SMF and a highly nonlinear MOF (NMOF) was done. Besides the backward-pump scheme as shown as in Ref. 9, forward and bidirectional pump schemes, as well as two NMOF types have been considered in this paper for the first time to our best knowledge. The experimental results indicate that the optical signal-to-noise ratio (OSNR) of the amplifiers with the three pump schemes are all improved when the NMOFs are placed at the end of the link, which is different from the results in Ref. 9 that the OSNR was improved when the NMOF was placed at the beginning of the link. The experimental analysis why the results are different is given in this paper.

2. EXPERIMENTAL CONFIGURATION

HFRAs with forward-pumped, backward-pumped, and bidirectional-pumped schemes as shown in [Figs. 1(a)–1(c)], respectively, are experimentally investigated. The three fiber-span configurations as shown in Figure 1(d) in every pump schemes are considered, respectively. In the span configuration of Case 1, the Raman gain medium consists of first a 25-km SMF and then a section of NMOF, that is, the NMOF is placed at the end of the span. In Case 2 configuration, only the 25-km SMF is used. In Case 3 configuration, the NMOF is placed at the beginning of the span. In order to investigate the effect of the NMOF with different parameters on the performance of the Raman amplifiers, two types of NMOF with different parameters and length were used in our experiment. Their cross-sectional scanning electron micrograph images are shown in Figures 1(e) and 1(f). The NMOF1, as shown in Figure 1(e), is fabricated by Blazephotonics Company (NL-2.4–800). Its core diameter is $\sim$2.4 μm, zero chromatic dispersion wavelength is at $\sim$800 nm, and 70 m of the fiber was used in the experiment described here. The nonlinear coefficient γ of the guided mode at 1550 nm in this fiber is about 36 W^{-1} km^{-1}. The attenuation

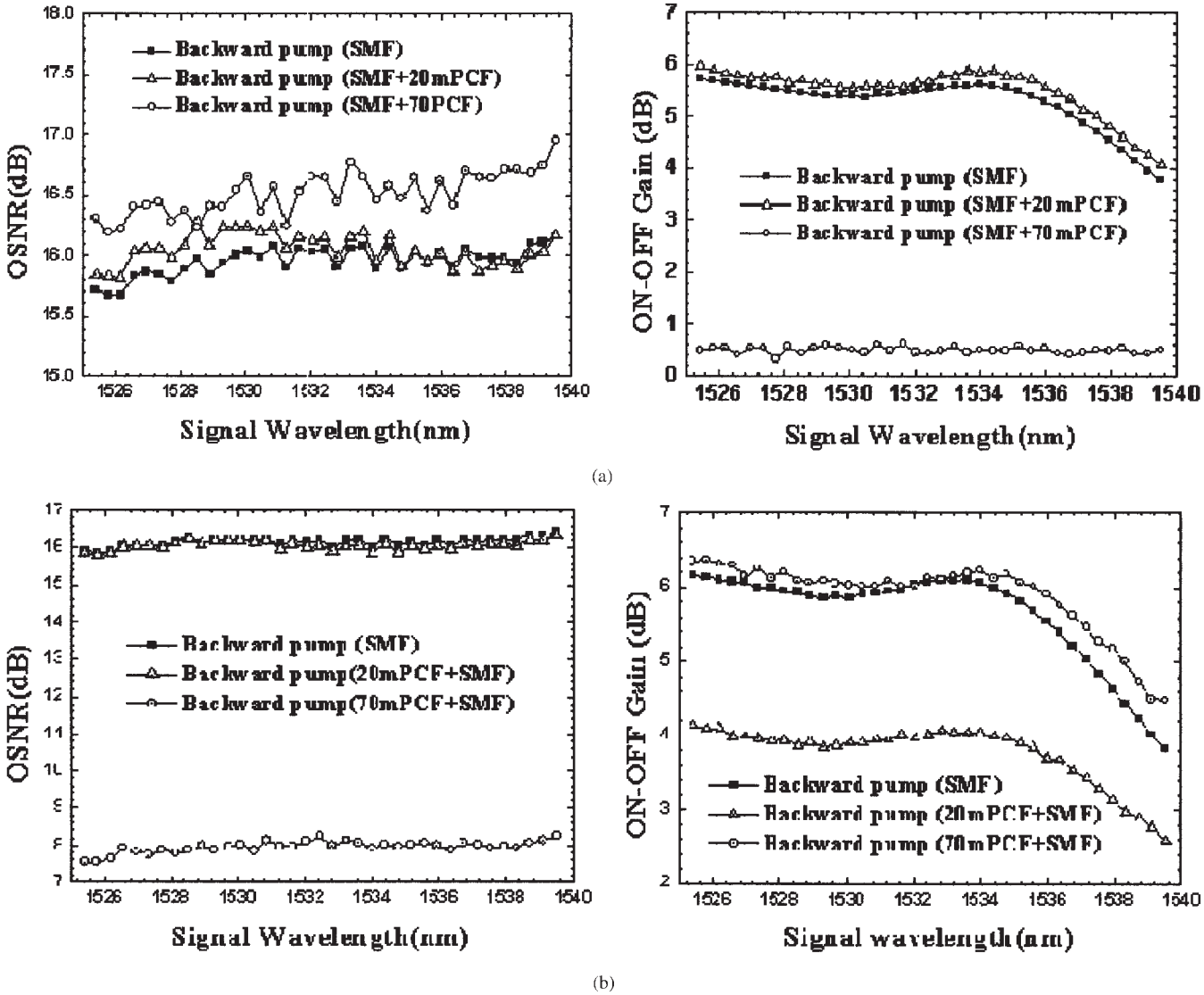

Figure 3 (a) Performance comparison between Case 1 and Case 2 for the backward-pumped configuration (the pump power is 327 mW). (b) Performance comparison between Case 3 and Case 2 for the backward-pumped configuration (the pump power is 365 mW)

coefficient of this fiber is about 40 dB km^{-1} at 1550 nm. Another section of NMOF (NMOF2), as shown in Figure 1(f), is fabricated by Crystal Fiber A/S. Its core diameter is ~2.1 μm, zero chromatic dispersion wavelength is at near 1550 nm, and 20 m of the fiber was used in our experiment. The nonlinear coefficient γ of the guided mode at 1550 nm is about 11 W^{-1} km^{-1}. The provided attenuation coefficient is about 9 dB km^{-1} at 1550 nm. The two sections of NMOF are both spliced to SMF via an intermediate fiber by the manufacturers. The total insert loss (including the loss of the two splicing points and the fiber transmission loss) at 1530 nm wavelength is measured to be ~11.6 dB for the 70-m NMOF1 and ~1.3 dB for the 20-m NMOF2. Comparing with the NMOF2, the NMOF1 has the higher loss. One reason is the less air-hole layers in this fiber induce higher loss. Another reason is the splicing loss between this fiber and SMF (more than 4 dB for one splicing point) is higher than that of NMOF2. Two Raman pumping modules, which were both multiplexed depolarized semiconductor lasers operating at the wavelength of 1427 nm, were used. The pump module 1 and 2 deliver a maximum power of ~365 and ~327 mW, respectively. The pump lights are coupled in the Raman gain fibers via two 1427/1527 nm wavelength division multiplexing couplers. A small signal source with 37 channels varied from 1525.425 to 1539.525 nm, at about 0.4 nm wavelength spacing, was used for the input measurement signal. The signal input power for every channel is about −30 dBm. The gain and OSNR characteristics are directly measured via an Agilent 86142B optical spectrum analyzer with a resolution of 0.06 nm.

3. EXPERIMENTAL RESULTS AND DISCUSSION

The on–off gain and OSNR spectra comparison between Case 1 (or Case 3) and Case 2 for the three pump schemes is given in Figures 2–4, respectively. The left figures of Figures 3(a) and 4(a) [or Figs. 3(b) and 4(b)] are the OSNR spectra comparison between Case 1 (or Case 3) and Case 2. The right figures are the corresponding on–off spectra comparison. Seen from the experimental results of the OSNR spectra, the OSNRs obtained in our experimental conditions are strongly dependent on the position of the NMOFs. Comparing with the distributed FRAs with only the 25-km SMF (Case2), the OSNR performances of the amplifiers for the three pump schemes are all improved when the NMOFs are placed at the end of the span [seen from the left figures of Figs.

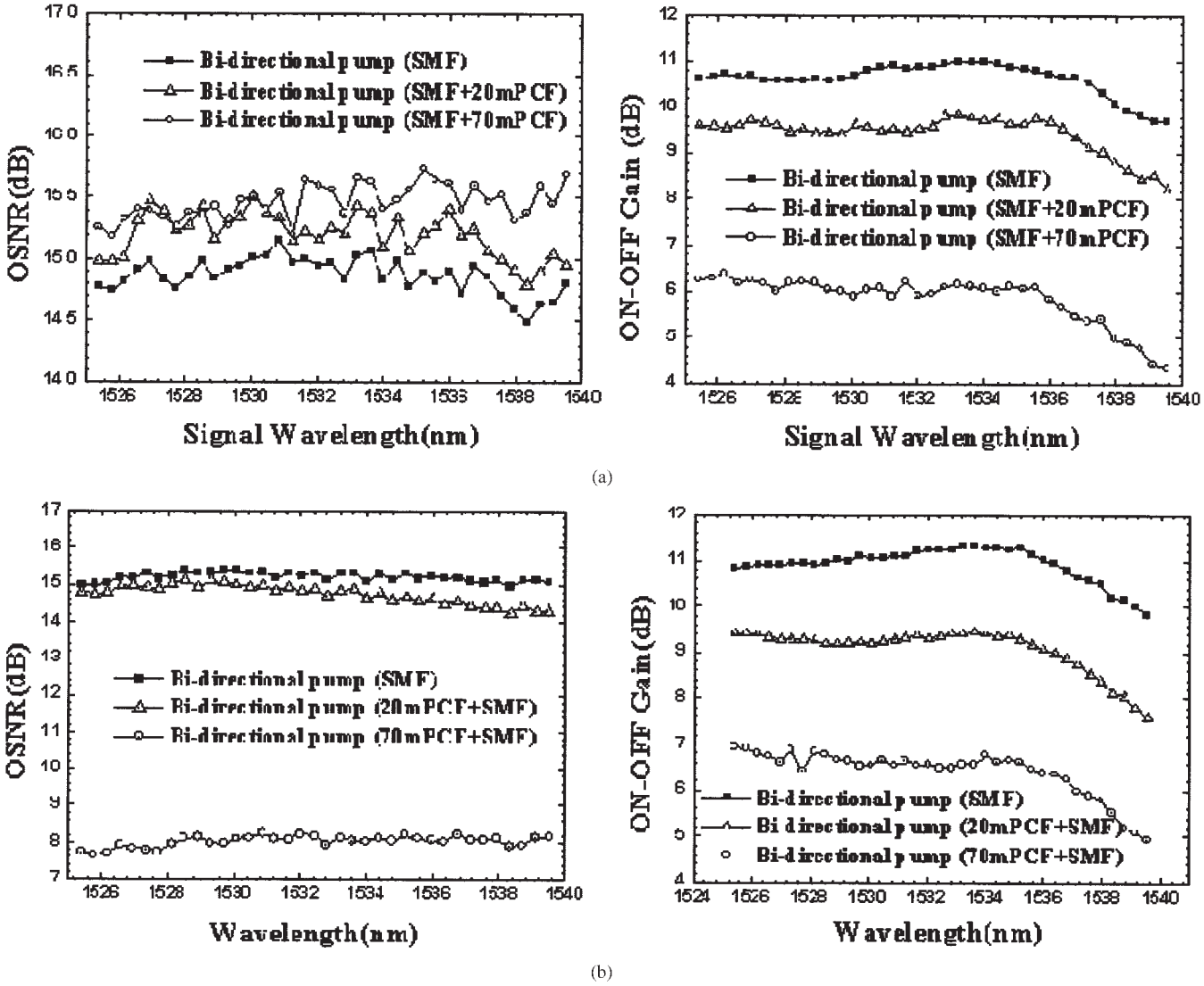

Figure 4 (a) Performance comparison between Case 1 and Case 2 for the bidirectional-pumped configuration (the forward pump power is 365 mW, the backward pump power is 327 mW). (b) Performance comparison between Case 3 and Case 2 for the bidirectional-pumped configuration (the forward pump power is 327 mW, the backward pump power is 365 mW)

2(a) and 4(a)], where the OSNRs for inserting 70-m NMOF1 are improved more than those for inserting 20-m NMOF2. A maximum increase in OSNR of at least 0.5 dB is obtained when inserting the 70-m NMOF2 at the span end, while the OSNRs all become worse when the NMOFs are placed at the beginning of the span. The decrease in OSNR is dependent on the pump schemes and NMOFs. For the forward pump configuration, the OSNR performance of inserting the 20-m NMOF2 is worse than that of inserting the 70-m NMOF1. For the backward and bidirectional pump configurations, however, the contrary results are seen that the OSNRs of inserting the 70-m NMOF1 are dramatically reduced and the maximum decrease is more than 7 dB. The experimental results obtained here for back-pumped scheme are different from the experimental results in Ref. 9, but are in good agreement with the theoretical analysis by Hainberger et al. [10]. Their simulation results also indicate that the OSNR is higher when a high nonlinearity fiber is placed at the end span than that of the fiber is placed at the beginning of the span for a certain pump power. This is due to the NMOFs have a larger Raman gain efficiency than the SMF, the closer the NMOFs are placed to the span end the higher the pumping efficiency becomes because the pump light still has a high power level [10]. Thus path-averaged signal power in the span configuration of Case 1 is higher than that of Case 3, which make higher OSNRs in the Case 1 span configuration be obtained.

Seen from the experimental results of on–off gain spectra (the right figures of Figures 2–4), the on–off gain spectra not only are dependent on the position of the NMOFs in the span, but also are related to the parameters of the NMOFs and the pump configurations. Comparing with the distributed FRA with only the 25-km SMF (Case2), the on–off gains are increased a little when the 20-m NMOF2 is inserted at the beginning of the span for the forward-pumped scheme [seen from the right figure of Figure 2(b)] and at the end of the span for the backward-pumped scheme [seen from the right figure of Figure 3(a)]. For the 70-m NMOF1, the on–off gains are lightly increased only when it is placed at the span beginning and is backward pumped [seen from the right figure of Figure 4(b)]. Furthermore, it is noted that the gain and OSNR performances are both improved for the case that the 20-m

TABLE 1 Performance comparison at 1530 nm wavelength between case 1 and case 3: On-Off gain (dB)/OSNR (dB)

	Forward pump	Backward pump	Bidirectional pump
S_{in}→SMF→70-m NMOF1→S_{out} (Case1)	5.42/15.99	0.51/16.66	5.89/15.51
S_{in}→70-m NMOF1→SMF→S_{out} (Case3)	0.57/15.42	6.03/8.03	6.56/8.09
S_{in}→SMF→20-m NMOF2→S_{out} (Case1)	3.99/15.94	5.56/16.24	9.63/15.5
S_{in}→20-m NMOF2→SMF→S_{out} (Case3)	5.53/15.28	3.90/16.2	9.2/15.01

NMOF2 is placed at the span end and is backward pumped [seen from the right figure of Figure 4(a)].

In order to compare the performance between Case 1 and Case 3, we give the on–off gain and OSNR data at 1530 nm wavelength for the two sections of NMOF in Table 1. Seen from those data, the OSNRs for the Case 1 are always higher than those for the Case 3. In other words, it has better OSNR performance when the NMOFs are placed at the span end. Seen from the on–off gain data, the contrary trend is obtained for the two types of NMOF. For forward and backward pump configurations, the farther the 70-m NMOF1 is placed to the pump source the higher the on–off gain is. For the 20-m NMOF2, however, the closer it is placed to the pump source the higher the on–off gain is. For bidirectional pump configuration, the higher on–off gain is obtained for the Case 3 configuration of the 70-m NMOF1 and the Case 1 configuration of the 20-m NMOF2. This is mainly caused by the different insertion loss of the two types of NMOF at the pump laser wavelength. For 70-m NMOF1, when it is placed close to the pump source, its insertion loss is so large (>10 dB) that the pump power after it is reduced dramatically and the pump power injected into the main Raman gain medium (the SMF) is very low. Even though the NMOF1 has large Raman gain efficiency, the large insertion loss at the pump wavelength causes impairment. Therefore, for the forward and backward pump configurations, when the pump power injects first the 70-m NMOF1 then the 25-km SMF, the on–off gain is very low (only 0.57 and 0.51 dB). Whereas, when the pump power injects first the 25-km SMF then the NMOF1, the large on–off gain mainly results from the pumped SMF. For the 20-m NMOF2, however, its insertion loss at pump wavelength is small. The on–off gains for all configurations result from the interaction of the 25-km SMF and the 20-m NMOF2. In other words, the large Raman gain efficiency of the 20-m NMOF2 plays important role in the hybrid-fiber Raman amplifiers with the different pump configurations.

4. CONCLUSION

In this paper, the OSNR and on–off gain performances of the HFRAs were experimentally investigated in detail. Three pump schemes and span configurations, as well as two NMOF types were considered. The influence of the NMOF presence on the OSNR and on–off gain values was analyzed. The experimental results indicate that the OSNRs of the amplifiers are strongly dependent on the position of the NMOFs. The OSNRs are always improved when the NMOFs are placed at the end of the span, whereas the on–off gains not only are dependent on the position of the NMOF in the span, but also are related to the fiber loss, fiber length, and pump configuration. Furthermore, comparing with the span configuration of only having the 25-km SMF, the gain and OSNR performances could both be improved when the 20-m NMOF is placed at the span end and is backward pumped. The experimental results obtained in this paper are also applicable to the dispersion-managed Raman-amplified system with a section of high nonlinearity fiber as dispersion compensator.

ACKNOWLEDGMENT

This work is supported by the State Key Development Programme for Basic Research of China (Grant No. 20003CB314906) and the National Natural Science Foundation of China (Grant No. 60407005).

REFERENCES

1. T.A. Birks, J.C. Knight, and P.S.J. Russell, Endlessly single-mode photonic crystal fiber, Opt Lett 22 (1997), 961–963.
2. A.L. Gaeta, Nonlinear propagation and continuum generation in microstructured optical fibers, Opt Lett 27 (2002), 924–926.
3. K.P. Hansen, Dispersion flattened hybrid-core nonlinear photonic crystal fiber, Opt Express 11 (2003), 1503–1509.
4. V. Finazzi, T.M. Monro, and D.J. Richardson, Confinement loss in highly nonlinear holey optical fibers, in Proceedings of Optical Fiber Communications Conference ThS 4, Southampton Univ., UK, 2002, pp 524–525.
5. J. Nilsson, R. Selvas, W. Belardi, J.H. Lee, Z. Yusoff, T.M. Monro, and D.J. Richardson, Continuous-wave pumped holey fiber Raman laser, Proceedings of Optical Fiber Communications Conference WR 6, Southampton Univ., UK, 2002, pp 315–317.
6. Z. Yusoff, J.H. Lee, W. Belardi, T.M. Monro, P.C. Teh, and D.J. Richardson, Raman effects in a highly nonlinear holey fiber: Amplification and modulation, Opt Lett 27 (2002), 424–426.
7. M. Fuochi, E. Poli, S. Selleri, A. Cucinotta, and L. Vincetti, Study of Raman amplification properties in triangular photonic crystal fibers, J Lightwave Technol 21 (2003), 2247–2254.
8. M. Bottacini, F. Poli, A. Cucinotta, and S. Selleri, Modeling of photonic crystal fiber Raman amplifiers, J Lightwave Technol 22 (2004), 1707–1713.
9. C. Zhao, Z. Li, X. Feng, C. Lu, W. Jin, and M. S. Demokan, Effect of a nonlinear photonic crystal fiber on the noise characterization of a distributed Raman amplifier, IEEE Photon Technol Lett 17 (2005), 561–563.
10. R. Hainberger, T. Hoshida, T. Terahara, and H. Onaka, Comparison of span configurations of Raman-amplified dispersion-managed fibers, IEEE Photon Technol Lett 14 (2002), 471–473.